Phys Chem Minerals (2003) 30: 59–68
DOI 10.1007/s00269-002-0290-2

ORIGINAL PAPER

A. P. Shpak · E. A. Kalinichenko · A. S. Lytovchenko
I. A. Kalinichenko · G. V. Legkova · N. N. Bagmut

The effect of γ-irradiation on the structure and subsequent thermal decomposition of brucite

Received: 22 April 2002 / Accepted: 6 November 2002

Abstract The effect of γ-irradiation on the structure, phase composition and kinetics of isothermal decomposition of natural textural brucite $Mg(OH)_2$ has been investigated by Mn^{2+} electron paramagnetic resonance (EPR), proton magnetic resonance (PMR), X-ray diffraction (XRD) and weight loss methods. Starting from a 10^6-Gy dose, γ-irradiation (^{60}Co, 13.8 Gys^{-1}) is found to stimulate the formation of a new phase in the brucite structure, namely basic magnesium carbonate. The carbonate phase is assumed to form in brucite under γ-irradiation accordingly to the scheme $Mg(OH)_2 \xrightarrow[-H_2O]{} MgO \xrightarrow[+CO_{2(atmosph)}]{} MgCO_3$ (in the brucite structure). There is also a possibility that γ-irradiation forms particles with high reaction ability, CO_2^- radicals and/or CO molecules, which can react with the brucite structure. Preliminary γ-irradiation (9.75×10^7 Gy) slows down the subsequent isothermal dehydroxylation of natural brucite, which can be explained by the formation of the new carbonate phase in the $Mg(OH)_2$ structure. Dehydroxylation kinetics of both original and irradiated samples are interpreted by a two-stage nucleation model at 623, 648, 673, 698 and 723 K. The reaction rate is limited by the first nucleation stage rate (proton transition from an OH group near the reaction interface on a freed vacant orbital of an oxygen ion of the OH group in the nearest elementary cell, i.e., formation of a structured water molecule). The second-stage rate (water molecule removal from the structure and proton migration from the residual hydroxyl inside the structure) is about 1 order of magnitude higher. The activation energy of the limiting stage is 194 and 163 kJ mol^{-1} for the original and irradiated samples, respectively. Non-linear Arrhenius dependencies for the first-stage rate constants are related to the potential barrier reduction due to thermal fluctuations of large structural zones (with radii of about 20 and 81 Å in original and irradiated samples, respectively), whose ions form this barrier.

Keywords Brucite · γ-Irradiation · Mn^{2+} EPR · Dehydroxylation

A. P. Shpak · G. V. Legkova
Physics and Technology Institute,
'KPI' National Technical University, Kiev, Ukraine

E. A. Kalinichenko (✉) · A. S. Lytovchenko · I. A. Kalinichenko
N. N. Bagmut
Institute of Geochemistry, Mineralogy and Ore Formation,
The National Academy of Sciences, Kiev, Ukraine
34 Palladin avenue, Kiev 03142, 03680
e-mail: pochta@online.com.ua
Tel.: 38-044-4443160
Fax: 38-044-4441270

Introduction

Exposure of solids to high-energy radiation is known to result in radiation-induced defects and at large doses even leads to destruction of other phases (Semeshko et al. 1975; Brown et al. 1980; Nikiforov et al. 1991; Clozel et al. 1994; Grigoriev and Trakhtenberg 1996; Wang et al. 1998; Weber et al. 1998; Belloni et al. 2000; Gu et al. 2000; Gournis et al. 2001; Lutoev et al. 2001; Sorieul et al. 2001). At the same time, various complex, heterogeneous and composite systems with desirable properties can be created using irradiation (Michalik et al. 1999; Young 1999; Belloni et al. 2000; Gournis et al. 2001; Mohmel et al. 2002). Impurities and crystalline order profoundly affect radiation-induced processes (Brown et al. 1980; Nikiforov et al. 1991; Clozel et al. 1994; Belloni et al. 2000; Gournis et al. 2001; Sorieul et al. 2001).

The objective of this work was the study of the γ-irradiation effect on the structure, phase composition and kinetics of isothermal decomposition of natural textural brucite, magnesium hydroxide. The $Mg(OH)_2$ structural motive is typical for many layered and banded structures (serpentines, talc, chlorites etc.), which are widely used, in particular in order to create new materials with desired properties (absorbents, ion-exchange media, catalysts etc.) (Rothon 1999; Zviagina 2000;

McKelvy et al. 2001; Béarat et al. 2002; Mohmel et al. 2002 etc.) and to solve problems in the processing and isolation of various industrial wastes, among them CO_2 (Butt et al. 1996; McKelvy et al. 2001; Béarat et al. 2002 etc.) and radioactive wastes (Samodurov et al. 1999; Zviagina 2000 etc.). Therefore, brucite can be regarded as a model material to study structures with brucite or brucite-like layers, in particular, to study mechanisms of destruction, interaction with various substances and accumulation of defects of different nature (including radiation-induced), as well as the estimation of stability to external influences and the development of new materials (Brown et al. 1980; Wengeller et al. 1980; McKelvy et al. 2001; Béarat et al. 2002).

In some cases, preliminary irradiation accelerates thermal decomposition of solids, in others it slows it down. The process mechanism is believed to remain unchanged, and the observed acceleration is caused by new structural defects which are nucleation centres, and the slowing down, as a rule, is explained either by the mechanism itself (namely the formation of many intermediates and the influence of the removal rate of gaseous products) or by formation of new bonds in the structure (Semeshko et al. 1975; Brown et al. 1980; Nikiforov et al. 1991; Belloni et al. 2000). The number of radiation-induced defects in layered OH-bearing minerals can be on the order of 10^{18} g^{-1}, and this can, to a certain degree, affect the subsequent mineral thermal decomposition. However, concentration of radiation-induced defects decreases during heating, as some types of defects recombine at rather low temperatures (even though others are stable up to the temperatures when dehydroxylation begins) (Nikiforov et al. 1991; Clozel et al. 1994; Lutoev et al. 2001; Sorieul et al. 2001).

Kinetics and mechanism of natural brucite dehydroxylation (structural OH group destruction) were widely studied by various techniques; however, the atomic-level nature of this process and its special features under various external conditions are still not clear and require further investigation (Brown et al. 1980; Wengeller et al. 1980; Butt et al. 1996; McKelvy et al. 2001; Béarat et al. 2002; Masini and Bernasconi 2002 etc.).

Brucite dehydroxylation is usually preceded by certain reversible imperfections in structure – detachment of a small number of protons (10^{13} mol^{-1}) from OH groups, and formation of structured water molecules which are centres of product nucleation (Wengeller et al. 1980). In sheet OH-bearing minerals, in particular in brucite, there are two possible mechanisms of proton transfer (Wengeller et al. 1980): mobile H^+ protons transfer [the activation energy of them appearance, U_{act}, is approximately equal to the proton potential barrier height – ~2.1 eV for $Mg(OH)_2$] and "slow" $H^\bullet$ protons transfer (an O^{2-} state displacement through a crystal with $U_{act} \sim 0.87$ eV for $Mg(OH)_2$ – an O^{2-} ion on a hydroxyl site takes a proton from the nearest OH group). A vacant orbital of an oxygen ion of a hydroxyl group in brucite can only occur on crystal boundaries or near structural defects (D'Arco et al. 1993). Accordingly, the nucleation centres usually at first form on the edges or surfaces of crystallites and then on the reaction interface (Brown et al. 1980; Wengeller et al. 1980; Butt et al. 1996; McKelvy et al. 2001; Béarat et al. 2002; Masini and Bernasconi 2002). MgO molar volume being half that of $Mg(OH)_2$, the mineral structure is friable on the reaction interface and in the zone of the formed product, so that structured water molecules are removed from small crystallites sufficiently quickly (Brown et al. 1980; Wengeller et al. 1980; Butt et al. 1996; Chizhik and Sidelnikov 1998; McKelvy et al. 2001; Béarat et al. 2002). In such a case, at high enough temperatures, the reaction interface moves into small crystallites with the rate generally determined by the MgO nucleation rate on that interface (Brown et al. 1980; Wengeller et al. 1980; Chizhik and Sidelnikov 1998), then the distinct MgO/$Mg(OH)_2$ reaction interface forms (McKelvy et al. 2001). The dehydroxylation kinetics of small crystallites usually obeys a first-order law and that of large crystallites a contracting sphere model; the activation energy of brucite dehydroxylation is about 150–160 kJ mol^{-1} (Brown et al. 1980; Butt et al. 1996; McKelvy et al. 2001).

Experimental

Natural brucite as platy crystallites of 10^{-5} m in radius and 10^{-6} m thickness was taken for the research. The impurities in this mineral do not exceed several tenths of a percent. The brucite elementary cell is trigonal ($a = b = 3.12$ Å, $c = 4.73$ Å), and its structure consists of $Mg(OH)_2$ layers: Mg^{2+} ions are located in the (001) plane, O^{2-} ions at 0.22**c** distance above and below the (001) plane and protons along the **c** axis at 0.98 Å distance from oxygen ions. Each Mg^{2+} ion is surrounded by six O^{2-} ions situated at the corners of a regular octahedron (Deer et al. 1962).

Samples were exposed to γ-irradiation with ^{60}Co (13.8 Gy s^{-1}) at room temperature in air and set in D_2O in glass capsules. The exposure doses were 10^4, 10^6, $D_{max} = 9.75 \times 10^7$ Gy for samples in air and 10^4, 10^6, 10^7, $D_{max} = 9.75 \times 10^7$ Gy for samples in D_2O.

Methods

Electron paramagnetic resonance (EPR) was the basic research method. Additionally, X-ray diffraction (XRD), proton magnetic resonance (PMR) and weight loss methods were used. The EPR spectra were recorded by a RE-1306 spectrometer (3-cm range), PMR spectra by RN-2301 spectrometer at $\nu_0 = 16$ MHz. All spectra were recorded at room temperature.

To study dehydroxylation kinetics of original and γ-irradiated (9.75×10^7 Gy) brucite, the relative weight loss of a sample was measured after isothermal heating at $T = 623$, 648, 673, 698 or 723 K in air during time t: $\sigma_T^{w.l.}(t) = m(t)/m(t=0)$. A dehydroxylation degree, $\alpha(t)$, was determined as the relative loss of OH groups and calculated by $\sigma_T^{w.l.}(t)$ data, using a calibration curve (Fig. 1), plotted by PMR data, σ^{PMR} (similarly to the description by Kalinichenko et al. 1997):

$$\alpha(t) = 1 - N_{OH}(t)/N_{OH}^0 = 1 - \sigma^{PMR}(t), \quad (1)$$

where $N_{OH}(t)$ is the number of structural OH groups in a sample at time t, and $N_{OH}^0 = N_{OH}(t=0)$.

The $\alpha(t)$ determination error did not exceed 3.5% (Kalinichenko et al. 1997).

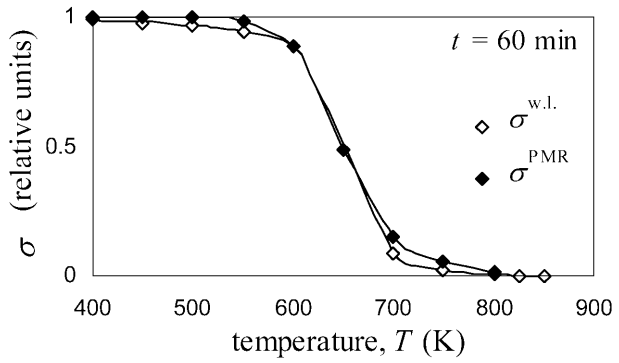

Fig. 1 Number of structural OH groups in brucite after 60 min isothermal heating on evidence from weight loss (*open diamonds*) and PMR data (*closed diamonds*)

Results and discussion

Spectroscopy data

The EPR spectrum of the original sample (Fig. 2a) shows the sextet of lines *1*, associated with Mn^{2+} impurities (~0.06% Mn^{2+} on the evidence of spectral analysis) in the $Mg(OH)_2$ lattice (Mn^{2+}:$S_{Mn^{2+}} = 5/2$, $I_{Mn^{2+}} = 5/2$). The spectrum parameters are practically the same as those determined by Altshuler and Kozyrev (1972): $g_{eff} = 1.9995 \pm 0.0005$ and $A = 9.16$ mT. The γ-irradiation causes a considerable decrease in both the peak (I_{peak}), and integrated intensities of the Mn^{2+} EPR sextet (Fig. 3). These intensities were estimated by the first (low-field) component. Additionally, in the EPR spectrum of the sample irradiated with the maximal dose, D_{max}, there appear two new sextets of lines 2–2 and, in the $g \approx 2$ region, a single line 3 with $\Delta B = 4.4$ mT (Fig. 2b).

The 2–2 lines were identified by express EPR mineralogical phase analysis of carbonates (Krutikov 1997). The effective g values of all Mn^{2+} EPR spectra components for MgO, $Mg(OH)_2$ and $MgCO_3$ (which was presumed to occur in the irradiated sample) were determined (Table 1). The values obtained are exact enough: e.g., the differences in g_{eff} for calcite determined in this research and taken from Krutikov (1997) are within experimental error (Table 1). The two sextets of EPR lines in carbonates appear due to the different anisotropy of **g** and **A** tensors. Table 1 shows that the g_{eff} values of the 2–2 lines have the highest magnitudes of the indicated compounds and are almost equal to the g_{eff} of carbonates. At the same time, data given in Table 1 shows that the new sextet of the Mn^{2+} EPR lines of a carbonate phase cannot be associated with the $MgCO_3$ phase.

To refine the obtained data, XRD patterns and PMR spectra were recorded for the original and irradiated brucite exposed to the maximal dose (Fig. 4) and the weight losses of these samples were measured on heating.

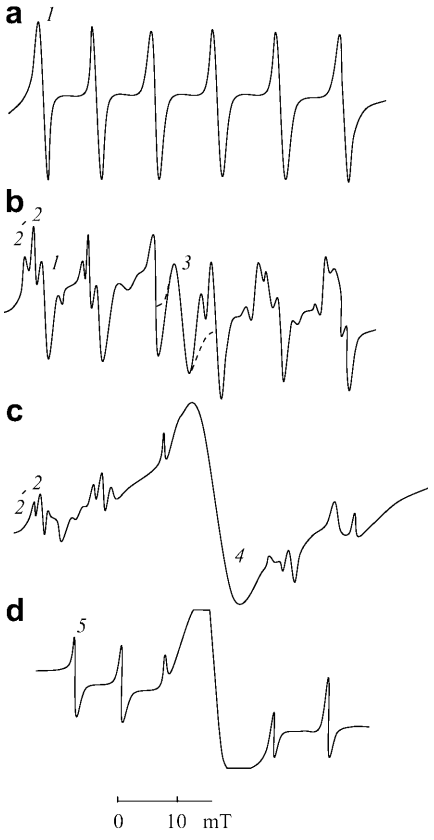

Fig. 2a–d Mn^{2+} EPR spectra of original brucite (**a**). Sample irradiated with D_{max} dose (**b**). Sample irradiated with D_{max} dose and then annealed at 623 K (**c**) and 1073 K (**d**). Changes in the Mn^{2+} EPR spectrum of natural brucite annealed at 623 and 1073 K are similar to **c** and **d**. *1* Mn^{2+} in $Mg(OH)_2$; *2–2* Mn^{2+} in the carbonate phase; 3 CO_3^- centres; *4* Fe^{3+}; *5* Mn^{2+} in MgO

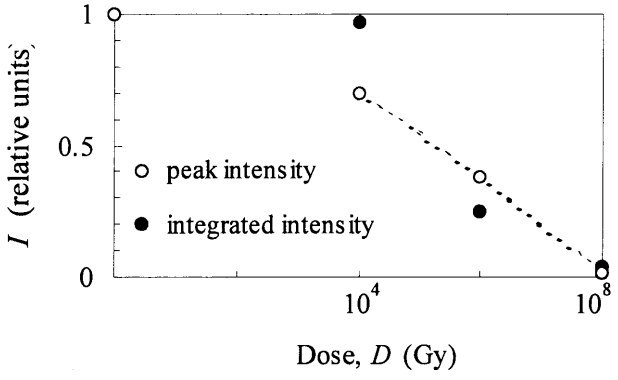

Fig. 3 Peak (*open circles*) and integrated (*closed circles*) intensities of the sextet of the Mn^{2+} EPR spectrum lines of $Mg(OH)_2$ versus γ-irradiation dose

The XRD pattern of the original sample shows the very small β-Fe_2O_3 peak in addition to basic phase reflections, and the XRD pattern of the irradiated sample shows the new diffraction reflection at $d/n = 2.82$ Å (Fig. 4a). This peak is specific for carbonate phases (Mikheev 1957). This result supports the EPR data on the new carbonate phase formation. The content of the

Table 1 Effective g values[a] of extremes of six groups of Mn^{2+} ions HFS lines in EPR spectra of magnesium carbonates, MgO and $Mg(OH)_2$

Mineral	Control point[b]	g^{a}_{eff}					
		1	2	3	4	5	6
MgO[c]	i.p.	2.1426	2.0874	2.0336	1.9812	1.9302	1.8805
MgO[d]	i.p.	2.1417	2.0873	2.0336	1.9809	1.9318	1.8809
$Mg(OH)_2$[c]	max	2.1490	2.0916	2.0359	1.9811	1.9313	1.8767
$CaCO_3$[c]	max	2.1579	2.0971	2.0394	1.9818	1.9278	1.8745
	min	2.1541	2.0922	2.0340	1.9759	1.9197	1.8651
$CaCO_3$[d]	max	2.1570	2.0967	2.0388	1.9822	1.9272	1.8740
	min	2.1517	2.0911	2.0325	1.9749	1.9185	1.8647
$MgCO_3$[d]	max	2.1565	2.0975	2.0385	1.9850	1.9280	1.8755
	min	2.1460	2.0860	2.0295	1.9730	1.9171	1.8635
$Mg(OH)_2$[c,e]	max_{carb}[f]	2.1631	2.1032	2.0464	1.9879	1.9344	1.8815
	min_{carb}[f]	2.1541	2.0947	2.0365	1.9790	1.9250	1.8725
	max_{hydr}[g]	2.1515	2.0908	2.0382	1.9813	1.9300	1.8785
	min_{hydr}[g]	2.1458	2.0886	2.0319	1.9790	1.9250	1.8738

[a] g value measurement accuracy in the present work and Krutikov (1997) is ± 0.0005
[b] i.p., max and min = inflection, maximum and minimum points on the derivatives of the Mn^{2+} EPR lines
[c] Data obtained in the present work
[d] Data from Krutikov (1997)
[e] Brucite irradiated with the maximum dose
[f] carb = basic magnesium carbonate
[g] hydr = magnesium hydroxide

new phase (magnesium carbonate) can be estimated as approximately 5%, the sensitivity of the method being the same as for calcite (Pawlovski 1985).

The PMR spectrum of irradiated brucite shows the new component disappearing when the sample is heated up to 373 K (Fig. 4b). This component is specific for weakly bound water. The crystallohydrated water band was not detected in the spectrum.

The relative weight loss on heating, $\sigma^{w.l.}$, also suggests the appearance of the carbonate phase: $\sigma^{w.l.}$ of the original and D_{max} dose-irradiated samples is, respectively, 32.27% (31.03% theoretical value) and 36.83%, and after the $\sigma^{w.l.}$ elimination up to 373 K, 31.70 and 35.04%. EPR spectra show that the formed carbonate phase decomposes completely on heating the irradiated sample to 973 K (Fig. 5). Thus, assuming that the 3.34% relative weight loss in the 373–973 K temperature range is caused by the new phase impurity, the carbonate phase content (basic waterless magnesium carbon-

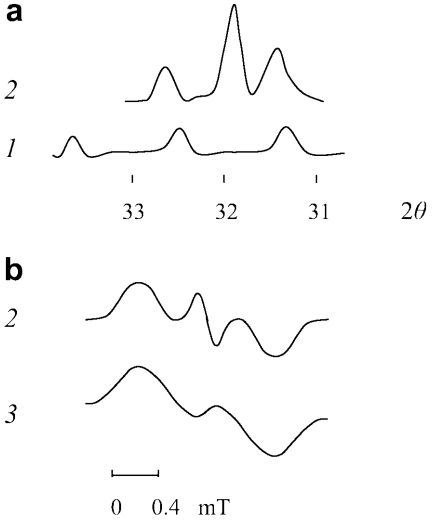

Fig. 4a, b XRD pictures (**a**) and PMR line derivatives (**b**) of original brucite (*1*), sample irradiated with D_{max} dose (*2*), sample irradiated with D_{max} dose and then annealed at 373 K (*3*)

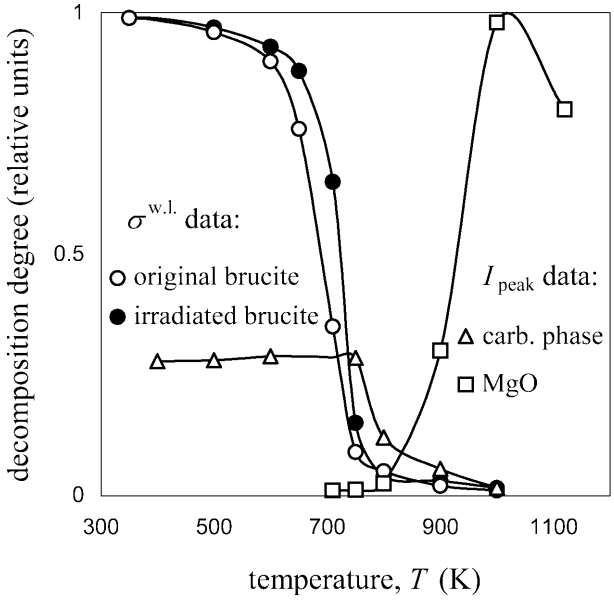

Fig. 5 Temperature dependencies of degree of decomposition (30 min heating) for original (*open circles*) and irradiated with D_{max} dose (*closed circles*) brucite by weight loss data, $\sigma^{w.l.}_T$, and for basic magnesium carbonate (impurity phase) (*triangles*) and MgO (*squares*) by EPR data, I_{peak} (relative peak intensities)

ate) is estimated as ~6%, which correlates well with the estimates obtained from the XRD data.

The formation of hydrous magnesium carbonate [$3MgCO_3 \cdot Mg(OH)_2 \cdot 3H_2O$] is not verified by XRD, EPR, PMR and weight loss data. The relative weight losses after heating in the 373–723 K range (hydroxyl groups destruction range) are virtually identical for the original samples and those irradiated with the D_{max} dose: 28.15 and 28.55%, respectively. The Mn^{2+} EPR spectrum of a carbonate phase also shows no appreciable changes (Fig. 5). At the same time, the difference in $\sigma^{w.l.}$ values exceeds 3% in the temperature range of the carbonate phase decomposition (800–900 K by EPR data, see Fig. 5).

Thus, γ-radiation exposure in brucite is followed by the formation of the same amount of basic magnesium carbonate, most probably $MgCO_3 \cdot Mg(OH)_2$ or $3MgCO_3 \cdot Mg(OH)_2$. Atmospheric carbon dioxide was the carbon source

$$2Mg(OH)_2 + \underset{(atm)}{CO_2} \xrightarrow{\gamma} MgCO_3 \cdot Mg(OH)_2 + H_2O. \qquad (2)$$

The products of $Mg(OH)_2$ transformation in nature are known to be different hydrocarbonates (Deer et al. 1962). This transformation process is apparently accelerated under γ-irradiation. Studies of the gas–solid $Mg(OH)_2$ carbonation mechanism are still in progress. Butt et al. (1996) and Béarat et al. (2002) suppose that a CO_2 molecule diffuses the inward structure instead of leaving H_2O molecules, then deforms and is adsorbed on the formed $MgO/Mg(OH)_2$ interface, where it reacts with MgO. Irradiation can be assumed to induce partial brucite dehydroxylation. Therefore, the carbonate phase in $Mg(OH)_2$ under γ-irradiation may form in the same way. There is also a possibility that γ-irradiation forms particles with a high reaction ability, CO_2^- radicals and/or CO molecules, which can react with the mineral structure.

The carbonate synthesis occurs immediately in the ionizing radiation field, rather than after radiation exposure: to take the maximum dose, the sample was exposed to γ-irradiation for almost 3 months. The EPR spectra were recorded several hours after irradiation, and the Mn^{2+} EPR spectrum did not change its shape with time (over about 2 years) under ambient conditions. This result indicates that carbonates should have high radiation stability, an assumption confirmed by EPR results with ^{60}Co irradiation of natural Ca–Mg carbonate simultaneously with $Mg(OH)_2$: even the maximum dose caused no noticeable changes in the Mn^{2+} EPR spectrum of Ca–Mg carbonate, and no signal of electron-hole centres was registered. Thus, there is no evidence for irreversible processes (chemical bonds breaking, loss of volatile components etc.) in carbonate under irradiation, and possible ionization disruptions recombine quickly without transforming the mineral structure.

Heating the original and irradiated brucite to 623 K causes, at first, considerable growth in intensity of the Mn^{2+} EPR sextet and then its sharp decrease (Fig. 6) as well as the appearance of a new EPR line 4 with $\Delta B = 10.4$ mT in the $g \approx 2$ region (Fig. 2c). The iron impurities are most likely responsible for this line. Further heating to 1073 K results in the appearance of a new sextet 5 (Fig. 2d), whose g_{eff} and A values correspond to those of the Mn^{2+} EPR spectrum for the MgO lattice (see Table 1). Figure 5 (squares) shows the temperature dependence I_{peak} of this sextet.

To elucidate the nature of the EPR line 3 in the $g \approx 2$ region (Fig. 2b), D_2O-irradiated samples were studied. The detailed spectrum analysis, similar to that in Fig. 2b, shows that this line is the superposition of signals caused by several types of carbonate centres, whose parameters are given in Table 2. The appearance of the CO_3^- centres formed from CO_3^{2-} ions undoubtedly relates to a carbonate phase, and indicates hydrocarbonate formation immediately under radiation exposure.

The hydroxide radiolysis processes are essentially accelerated under irradiation in a wet environment (D_2O). If $Mg(OH)_2$ phase destruction occurs in about the same way as under irradiation in air, the carbonate phase is formed more actively (see Table 3). Intensive growth of the Mn^{2+} EPR signal in the carbonate phase and a number of carbonate centres (CO_3^-, CO_2^-) are observed, and at the maximum dose the O^- centre appears. This centre is believed to be the analogue of such a centre in apatite and to form when hydroxide

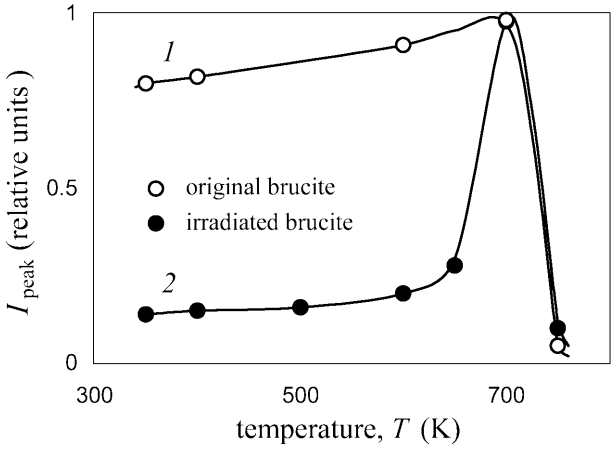

Fig. 6 Temperature dependencies (30 min heating) of relative peak intensities of the Mn^{2+} EPR spectrum lines of original (*open circles*) and with D_{max}-irradiated (*closed circles*) brucite

Table 2 Parameters of carbonate paramagnetic CO_3^- and CO_2^- centres and O^- oxygen centre in irradiated $Mg(OH)_2$

Centre	Mineral	$g\parallel$	$g\perp$
CO_3^-	$Mg(OH)_2$ in air	2.0180	2.0060
	$Mg(OH)_2$ in D_2O	2.0170	2.0055
	$CaCO_3$[a]	2.0162	2.0051
CO_2^-	$Mg(OH)_2$ in D_2O	1.9977	2.0039
O^-	$Mg(OH)_2$ in D_2O	2.001	2.055

[a] Data from Gilinskaya and Scherbakova (1975)

Table 3 Number of paramagnetic centres[a] in brucite, γ-irradiated in air and in D_2O by different irradiation doses

Dose, Gy	$Mg(OH)_2$ irradiated in air			$Mg(OH)_2$ irradiated in D_2O				
	Mn^{2+} in carb.ph.[b]	Mn^{2+} in $Mg(OH)_2$	CO_3^-	Mn^{2+} in carb.ph.[b]	Mn^{2+} in $Mg(OH)_2$	CO_3^-	CO_2^-	O^-
0	–	518	–	Minor	518	n/f[c]	n/f[c]	–
10^4	–	407	–					
10^6	Minor	208	–	1.2	240	n/f[c]	n/f[c]	–
10^7				9.3	10.8	17.2	40.3	–
9.75×10^7	4.1	6.6	16.1	4.4	3.5	55	18	1.9

[a] By EPR data in relative units
[b] carb.ph.-the carbonate phase
[c] n/f-not found

dehydroxylates under irradiation according to the scheme: $OH^- - OH^- - OH^- \rightarrow OH^- - O^- - OH^-$.

As mentioned above, γ-radiation causes a peak intensity decrease in the Mn^{2+} EPR lines sextet. This intensity is partially restored when samples are heated: the I^0_{peak} value in the original sample falls to 0.02 I^0_{peak} at D_{max} irradiation, and when the irradiated sample is heated at $T < 673$ K, the intensity increases to 0.17 I^0_{peak} only. Figure 6 demonstrates that the intensity grows in the 623–673 K range (curve 2), when dehydroxylation already occurs, and the intensity of the Mn^{2+} lines decreases as a result of brucite lattice transformations (curve 1).

The temperature dependence the intensity of the Mn^{2+} EPR lines in irradiated $Mg(OH)_2$ (Fig. 6) can be explained as follows. Under ionizing radiation, Mn^{2+} ions transform partially to the three-valent state: $Mn^{2+} - e^- \rightarrow Mn^{3+}$; correspondingly the intensity of the Mn^{2+} EPR lines falls. As, due to partial dehydroxylation, an oxygen ion of the water molecule moves from a crystal, an anion vacancy appears in the brucite structure. The intensity of the Mn^{2+} EPR lines is restored slightly by heating the irradiated sample at $T < 673$ K (Fig. 6). Therefore, it can be assumed that the knocked out electron is located in the same polyhedron oxygen vacancy, that is, the bound pair of $e^- - Mn^{3+}$ forms.

Thus, the thermal and radiation destruction of brucite is reflected differently in its Mn^{2+} EPR spectrum. When thermal dehydroxylation takes place, the decrease in the sextet intensity correlates completely with the degree of transformation $Mg(OH)_2$ in MgO (Figs 5, 6). The irradiation causes an appreciable reduction in Mn^{2+} EPR signal intensity; thus the carbonate phase formation is observed, but the MgO phase is not found (Fig. 2b). The thermal stability of the newly formed phase is less than that of natural magnesite: it is decomposed at about 770 K on the evidence of EPR (Fig. 5), in contrast to 923 K for the natural mineral (Deer et al. 1962). Figure 5 demonstrates that the initial and final stages of thermal decomposition of original and irradiated $Mg(OH)_2$ are the same, but the irradiated sample dehydroxylates appreciably more slowly when the process rate is maximal. A similar picture is observed on isothermal heating (Fig. 7).

Kinetics and mechanism of original and irradiated brucite dehydroxylation

To investigate a preliminary γ-irradiation effect on thermal decomposition of brucite, the isothermal dehydroxylation at 623, 648, 673, 698 and 723 K of the original and mineral irradiated with the D_{max} dose was studied.

As Fig. 7 shows, preliminary γ-irradiation slows down the subsequent isothermal $Mg(OH)_2$ dehydroxylation.

To determine the process mechanism, the experimental data were analyzed in several coordinate systems using the least-squares method. Taking into account published data on a possible mechanism of brucite dehydroxylation (Brown et al. 1980; Wengeller et al. 1980; Butt et al. 1996; McKelvy et al. 2001; Masini and Bernasconi 2002), the most probable kinetic models were considered: the contracting cylinder and sphere models, diffusion control, one- and two-stage nucleation and/or subsequent one-, two- or three-dimensional growth of nuclei formed in the disc crystallites (Brown et al. 1980).

The obtained kinetic data on thermal destruction of both the original and irradiated brucite at all investigated temperatures were best parameterized by the following two-stage nucleation model. As mentioned above, the brucite dehydroxylation elementary process (appearance of a stable product nucleus – an O^{2-} ion instead of two OH groups in one elementary cell) can be schematically presented as two consecutive reactions (Wengeller et al. 1980):

$$Mg(OH)_2[NB] \xrightarrow[+H^+]{k_1} H_2O - Mg - OH\ [NC] \xrightarrow[-H_2O,-H^\bullet \text{ or } -H^+]{k_2} Mg - O\ [NP], \quad (3)$$

where NB designates one elementary cell of brucite, NC one nucleation centre and NP one elementary cell of the product, MgO (one product nucleus). The concentration of H^+ ions, detached from OH groups before the onset of dehydroxylation and initiating the process, is about 10^{13} mol^{-1} (Wengeller et al. 1980). As mentioned above,

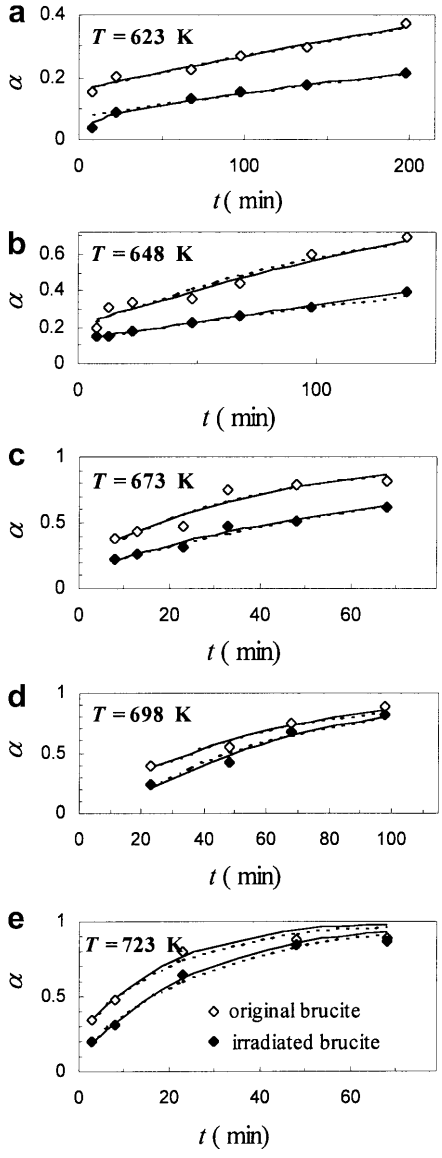

Fig. 7a–e Kinetics of isothermal dehydroxylation of original (*open diamonds*) and irradiated by D_{max} dose (*closed diamonds*) brucite at 623 K (**a**), 648 K (**b**), 673 K (**c**), 698 K (**d**) and 723 K (**e**). *Diamonds* correspond to experimental data; *solid curves* correspond to Eq. (4), *dotted curves* to Eq. (5)

small brucite crystallites dehydroxylate via relatively slow nucleation, leading to the distinct $MgO/Mg(OH)_2$ reaction interface. Thus, in the present case, it is possible to neglect the number of O–Mg–OH [NB$^{\bullet}$] elementary cells.

Assuming that each reaction in scheme (3) is an irreversible first-order reaction, it can be shown that the dehydroxylation degree in time t is equal

$$\alpha(t) = 1 - \frac{N_{OH}}{N^0_{OH}} = 1 - n_{NB} - n_{NC}/2 - n_{NB^{\bullet}}/2 \cong 1 + h_1 e^{-k_1 t} + h_2 e^{-k_2 t}, \quad (4)$$

where $n_{NB} = N_{NB}/N^0_{cells}$, $n_{NC} = N_{NC}/N^0_{cells}$, $n_{NB^{\cdot}} = N_{NB^{\cdot}}/N^0_{cells} \approx 0$, N_{NB}, N_{NC} and $N_{NB^{\cdot}}$ are the number of elementary cells of natural brucite NB, number of nucleation centres NC and elementary cells NB$^{\cdot}$, respectively, N^0_{cells} the number of all elementary cells in a sample at the initial point in time ($t = 0$), $h_1 = -n^0_{NB}(1+\kappa/2)$, $h_2 = -(n^0_{NC} - n^0_{NB}\kappa)/2$, $\kappa = k_1/(k_2 - k_1)$, $n^0_{NB} = n_{NB}(t = 0)$, $n^0_{NC} = n_{NC}(t = 0)$, k_1 and k_2 are rate constants of the first and second stages, respectively. Figure 7 (solid curves) demonstrates that Eq. (4) adequately describes dehydroxylation kinetics of both samples at all temperatures.

The obtained kinetic data can also be represented by a first-order equation, though with less accuracy (Fig. 7, dotted curves)

$$\alpha(t) = 1 - h_0 e^{-kt}, \quad (5)$$

where h_0 and k are experimental constants ($h_0 \approx 1$, $k \approx k_1$).

Equations of such a type are characteristic of dehydroxylation kinetics of small brucite crystallites (Brown et al. 1980). These equations can describe reactions proceeding by different mechanisms; for example, product nucleation according to the exponential law with/or subsequent growth of the nuclei that have appeared (Brown et al. 1980), diffusive slowing down in the removal of water formed when a reaction interface moves into a crystallite (Toussaint et al. 1963). Therefore, to establish the exact mechanism, additional data are required. However, in the present case, it can be explained by the noticeably higher second-stage rate over the first-stage rate at all temperatures, except for 698 K. At 698 K both stage rates are about the same (Fig. 8).

Figure 8 represents the dependencies of $\ln(k_1)$ and $\ln(k_2)$ versus $1/T$ for the investigated samples. Most probably, the second stage is a more complex process than is represented by scheme (3). However, its resulting rate is essentially higher than the first-stage rate (at all temperatures except for 698 K). Because of this, the obtained $\ln(k_2)$ values are given in Fig. 8 for comparison, and further consideration is given only to the first nucleation stage which limits the brucite dehydroxylation rate.

Figure 8 shows that γ-irradiation does not change the type of the $\ln(k_1)$ vs. $1/T$ dependence. The rate constants of the first nucleation stage decrease slightly (Fig. 8), although this stage activation energy, $U_{act,1}$, is reduced from 194 to 163 kJ mol^{-1} after γ-irradiation. Some reduction of the $U_{act,1}$ value can be due to the appearance of certain radiation-induced defects in the ideal mineral lattice.

In the context of the considered model of brucite dehydroxylation (scheme 3), the first nucleation stage is the structured water molecule formation near the $MgO/Mg(OH)_2$ interface. Wengeller et al. (1980) describe this process at the local level as follows. Mg^{2+} ion displacement, when the structure is transformed (McKelvy et al. 2001), leads to the appearance of a vacant orbital of an oxygen ion of the OH group near

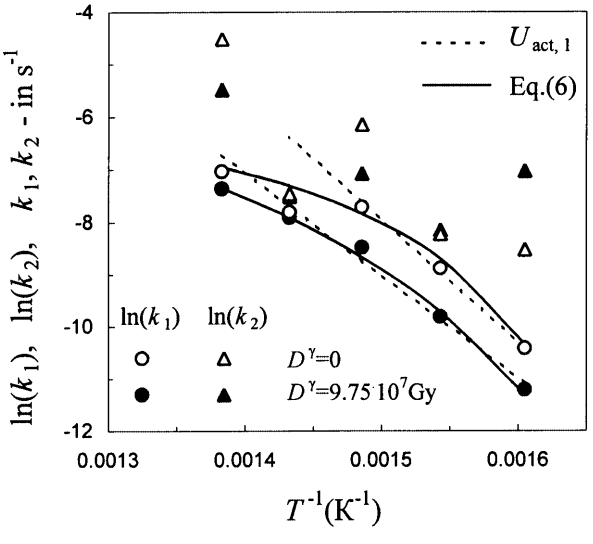

Fig. 8 Arrhenius plots for $\ln(k_1)$ (*squares*) and $\ln(k_2)$ (*triangles*) for original (*open symbols*) and irradiated with D_{max} dose (*closed symbols*) brucite. *Symbols* correspond to experimental data. *Solid curves* reflect $\ln(k_1)$ values as deduced from Eq. (6) with constants given in Table 4. Activation energies are calculated from the relevant slopes (*dotted lines*)

the reaction interface. In the neighbourhood of the interface the structure is already deformed to a certain extent. Therefore, most probably this vacant orbital is occupied by a proton from the nearest elementary cell. As a result, a structured water molecule is formed (Wengeller et al. 1980). The $U_{act,1}$ value obtained in the present work for the original mineral is of the same order as the dehydroxylation activation energy of small brucite crystallites ($\sim$160 kJ mol^{-1}, according to Brown et al. 1980) and is virtually the same as the activation energy of the appearance of free H^+ protons, that is approximately equal to the proton potential barrier height in this mineral, i.e., $\sim$2.1 eV (Wengeller et al. 1980). Thus, based on the features of dehydroxylation in small brucite crystallite at high temperatures (Brown et al. 1980; Wengeller et al. 1980; Chizhik and Sidelnikov 1998; McKelvy et al. 2001) and data obtained on the dehydroxylation kinetics of original and irradiated mineral at all investigated temperatures, it may be concluded that, determined by experimental data, the rate constant of the first nucleation stage is the rate constant of the elementary process of proton transition through the potential barrier between the next two structural OH groups near the reaction interface.

The dependencies $\ln(k_1)$ vs. $1/T$ for original and irradiated samples can be described by Eq. (Fig. 8, solid curves):

$$\ln(k_1) = C_1 + C_2/(C_3 + 1/T), \quad (6)$$

where C_1, C_2 and C_3 are constants (Table 4).

The analogous non-linear Arrhenius dependence was obtained for the rate constant of nucleation (the process of a proton transition between the two nearest OH groups) when muscovite dehydroxylation occurs (Kalinichenko et al. 1997). In the context of the present model of brucite dehydroxylation, the obtained dependence (Eq. 6; Fig. 8), can be explained similarly to Kalinichenko et al. (1997), namely by the mechanism features of the limiting stage. As shown by Goldansky et al. (1989), in solids at high temperatures a proton overcomes the barrier to the next potential well (onto the vacant orbital of the nearest OH group) when the height and width of this barrier decrease owing to thermal fluctuations of the structural ions shaping the barrier. In this case, Arrhenius dependence of the rate constant of proton transition through a potential barrier becomes non-linear at high enough temperatures and can be presented by Eq. (6) (Goldansky et al. 1989).

Similarly to the results of Kalinichenko et al. (1997), the parameters of anharmonic oscillator whose oscillations describe the oscillations of parameters of the proton structural potential barrier in brucite were numerically determined (Table 4). The proton was supposed to go from a structural OH group into the nearest elementary cell on the freed vacant orbital of the oxygen ion of the closest OH group along the straight line connecting two possible proton sites. The proton potential energy curve along the transition trajectory was approximated by two counter-Morse potentials taken from Martens and Freund (1976).

Table 4 shows that $Mg(OH)_2$ exposure to γ-irradiation causes an increase in this oscillator mass, i.e., the size of the structural zone whose ions shape the potential barrier. Moreover, the characteristic frequency of the fluctuations in the barrier shape, Ω, decreases. This fact

Table 4 Coefficients of Eq. (6) and parameters of the anharmonic oscillator whose oscillations correspond to oscillations of the proton structural potential barrier in brucite

Dose, Gy	C_1	C_2, 10^{-3} K^{-1}	C_3, 10^{-3} K^{-1}	$M\Omega^{2}$[a,b], J m^{-2}	M[a], 10^{-23} kg	Ω[b], 10^{11} s^{-1}	ζ_4[c], 10^{19} J m^{-4}	R[d], Å
0	−4.585	0.89	−1.76	2.03[e]	8.34[e]	1.56[e]	−4.43[e]	19.8[e]
9.75×10^7	−1.894	2.87	−1.91	0.630[e]	562[e]	0.106[e]	−0.473[e]	80.7[e]

[a] M Anharmonic oscillator mass
[b] Ω Frequency of its oscillations
[c] ζ_4 Anharmonic fourth order correlation
[d] R Radius of the structural zone which ions shape the proton potential barrier in brucite
[e] Barrier width is 3.25 Å (distance between two possible proton sites in structure without consideration for ions fluctuations), ΔU = −0.05 eV $\approx$ the asymmetry of the potential energy curve ($\Delta U = U_{initial} - U_{final}$ − difference in the energy levels between which the proton jumps)

can explain the rate decrease of the first nucleation stage in irradiated brucite, despite a certain reduction of the activation energy at this stage (see Fig. 8) – the frequency of appearance of such a barrier shape at which the proton transition is most probable (Goldansky et al. 1989) decreases by several times after irradiation (Table 4). This Ω decrease compensates for the increase in the rate constant due to $U_{act,1}$ reduction.

Thus, preliminary γ-irradiation causes a slowing down in the dehydroxylation of small brucite crystallites, which is due to a decrease in the rate of the limiting reaction stage (apparently the mineral structure becomes more stable as a result of the formation of a small amount of more thermostable carbonate phase). The decreasing number of possible centres of dehydroxylation onset (structural defects on crystallite surfaces) in the irradiated mineral, due to their participation in the partial dehydroxylation and formation of some carbonate phase on previous γ-irradiation, can also play a certain part.

Conclusions

By the methods EPR Mn^{2+}, PMR, XRD and weight loss it is shown that exposure of natural brucite to γ-irradiation results in the partial destruction of its structure and the formation of a basic waterless magnesium carbonate, $MgCO_3{\cdot}Mg(OH)_2$ or $3MgCO_3{\cdot}Mg(OH)_2$. The total output of brucite radiolysis products is approximately 5% for the absorbed dose of 9.75×10^7 Gy.

Preliminary γ-irradiation (9.75×10^7 Gy) slows down the subsequent isothermal dehydroxylation of natural brucite with Mn^{2+} impurities: the degree of dehydroxylation (at the same time) and the rate constant of the limiting stage are reduced. These facts can be explained by the formation of a new carbonate phase in the mineral structure. At the same time, the activation energy of this stage decreases from 194 to 163 kJ mol^{-1}, which can be due to defects in the ideal mineral lattice, formed as a result of γ-irradiation.

The kinetics of isothermal dehydroxylation of both the original and irradiated (9.75×10^7 Gy) brucite can be described by a two-stage nucleation model at all investigated temperatures (623, 648, 673, 698 and 723 K). The reaction rate is limited by the rate of the first nucleation stage – the process of a proton transition from the OH group near the reaction interface on the freed vacant orbital of the oxygen ion of the closest OH group in the elementary brucite cell (a structured water molecule formation). The rate of the second-stage (this molecule removal from the lattice and the proton migration from the residual hydroxyl into the structure) is about an order of magnitude higher than the rate of the first-stage . The rates of both stages for both samples at 698 K are about the same.

The brucite structure is not substantially transformed after γ-irradiation, as the dehydroxylation mechanism and the type of the Arrhenius dependencies for the rate constants of the nucleation stages do not change.

The non linearity of the Arrhenius dependencies for the rate constant of the first nucleation stage of original and irradiated $Mg(OH)_2$ at the temperatures investigated can be explained by the features of this mechanism stage. A proton overcomes the potential barrier to the closest OH group when the height and width of this barrier decrease due to thermal fluctuations of lattice ions shaping this barrier. These changes in the proton potential energy curve along the transition trajectory can be caused by oscillations (1.56×10^{11} s^{-1} and 1.06×10^{10} s^{-1} frequency) of large structural zones (8.34×10^{-23} kg and 5.62×10^{-21} kg mass) with radii of about 20 and 81 Å in the original and irradiated brucite, respectively.

Acknowledgements This study was supported by INTAS Project 01–2166.

References

Altshuler SA, Kozyrev BM (1972) Electron paramagnetic resonance of intermediate groups elements compounds, in Russian Nauka Publ, Moscow

Béarat H, McKelvy MJ, Chizmeshya AVG, Sharma R, Carpenter RW (2002) Magnesium hydroxide dehydroxylation/carbonation reaction processes: implications for carbon dioxide mineral sequestration. J Am Cer Soc 85: 742–748

Belloni J, Delcourt MO, Houée-Lévin C, Mostafavi M (2000) Radiation chemistry. Annu Rep Prog Chem (C) 96: 225–295

Brown ME, Dollimore D, Galvey AK (1980) Reactions in the solid state. In: Bamford CH, Tipper CFH (eds) Comprehensive chemical kinetics, vol 22. Elsevier Scientific, Amsterdam

Butt DP, Lackner KS, Wendt CH, Conzone SD, Kung H, Lu YC, Bremser JK (1996) Kinetics of thermal dehydroxylation and carbonation of magnesium hydroxide. J Am Cer Soc 79: 1892–1898

Chizhik SA, Sidelnikov AA (1998) Kinetics of solid-state reactions with a positive feedback between reaction and destruction, part I. The quantitative model of the destruction front propagation, in Russian. RAN News, Chem Ser 4: 626–631 (Izvestiya Rossiyskoy Academii Nauk, Seriya khimicheskaya – Russian Academy Science News, Chemistry series)

Clozel B, Allard T, Muller J-P (1994) Nature and stability of radiation-induced defects in natural kaolinites: new results and a reappraisal of published works. Clays Clay Miner 42: 657–666

D'Arco P, Causà M, Roetti C, Silvi B (1993) Periodic Hartree-Fock study of a weakly bonded layer structure: brucite $Mg(OH)_2$. Phys Rev (B) 47: 3522–3529

Deer WA, Zussman RA, Howie J (1962) Rock-forming minerals, vol 5. Longmans, London

Gilinskaya LG, Scherbakova MYa (1975) Isomorphic replacements and structural disruptions in apatite by the electron paramagnetic resonance data. In: Apatite physics, in Russian. Nauka Publ, Siberian department, Novosibirsk, pp 7–63

Goldansky VI, Trakhtenberg LI, Fleurov VN (1989) Tunneling phenomena in chemical physics. Gordon and Breach Science, New York

Gournis D, Mantaka-Marketou AE, Karakassides MA, Petridis D (2001) Ionizing radiation-induced defects in smectite clays. Phys Chem Miner 28: 285–290

Grigoriev EI, Trakhtenberg LI (1996) Radiation-chemical processes in solid phase: theory and application, CRC Press, New York

Gu BX, Wang LM, Simpson PA, Minc LD, Ewing RC (2000) Radiation and thermal effects in zeolite-NaY. Materials Research Society Symposia Proceedings 608: 493–498

Kalinichenko EA, Litovchenko AS, Kalinichenko AM, Bagmut NN, Dekhtyaruk NT (1997) The study of the kinetics and the mechanism of dehydroxylation in muscovite by ESR on Fe^{3+}. Phys Chem Miner 24:520–527

Krutikov VF (1997) Electron paramagnetic resonance – the express mineralogical phase analysis method. In: Bakhtin AI (ed) Spectroscopy, X-ray analysis and crystallochemistry of minerals, in Russian. Kazan University Press, Kazan, pp 118–124

Lutoev VP, Yukhtanov PP, Potapov SS (2001) Isomorphic impurities and radiation defects of hydrous phyllosilicates. Proceedings 4th European Conference: Mineralogy and Spectroscopy, Paris, France, September 10th–14th, 2001. Bull Liaison SFMC 13 (3): 89–90

Martens R, Freund F (1976) The potential energy curve of the proton and the dissociation energy of the OH-ion in $Mg(OH)_2$. Phys Stat Sol 37a: 97–104

Masini P, Bernasconi M (2002) Ab initio simulations of hydroxylation and dehydroxylation reactions at surfaces: amorphous silica and brucite. J Phys Condens Matter 14: 4133–4144

McKelvy MJ, Sharma R, Chizmeshya AVG, Carpenter RW, Streib K (2001) Magnesium hydroxide dehydroxylation: in situ nanoscale observations of lamellar nucleation and growth. Chem Mater 13: 921–926

Michalik J, Yamada H, Sadlo J, Shimomura S, Takenouchi S, Uchida Y (1999) Paramagnetic silver clusters in sodalites with oxyanions. The 9th EUROCLAY Conference, Krakow, Poland, September 5th – 9th, 1999, Abstracts: 112

Mikheev VI (1957) Minerals determination by X-ray diffraction, in Russian. Gosgeoltekhizdat, Moscow

Mohmel S, Kurzawski I, Uecker D, Muller D, Gebner W (2002) The influence of a hydrothermal treatment using microwave heating on the crystallinity of layered double hydroxides. Crystallogr Res Technol 37: 359–369

Nikiforov AS, Kosareva IM, Savushkina MK (1991) The study of radiation thermal stability of aluminosilicate minerals. Russ J Phys Chem 65: 2210–2214

Pawlovski GA (1985) Quantitative determination of mineral content of geological samples by X-ray diffraction. Am Mineral 70: 663–667

Rothon RN (1999) Mineral fillers in thermoplastics: filler manufacture and characterisation. Adv Polymer Sci 139: 67–107

Samodurov V, Hach-Ali PF, Galindo A (1999) Pripyat trough palygorskite-bearing rocks for disposal of radioactive waste. The 9th EUROCLAY Conference, Krakow, Poland, September 5th–9th, 1999, Abstracts: 130

Semeshko AV, Sviridov VV, Schukin GL (1975) Ultraviolet radiation affect on cadmium hydroxide, in Russian. In: Kinetics and mechanism of chemical reactions in solid. Belorussian University Press, Minsk, pp 135–140

Sorieul S, Allard Th, Boizot B, Calas G (2001) Radiation-induced defects in montmorillonite. An EPR study. Proceedings of the 4th European Conference: Mineralogy and Spectroscopy, Paris, France, September 10th–14th, 2001. Bull Liaison SFMC 13 (3): 110

Toussaint F, Fripiat JJ, Gastuche MC (1963) Dehydroxylation of kaolinite. 1. Kinetics. J Phys Chem 67: 26–30

Wang LM, Wang SX, Gong WL, Ewing RC (1998) Temperature dependence of Kr ion-induced amorphization of mica minerals. Nucl Instr Meth Phys Res (B) 141: 501–508

Weber WJ, Ewing RC, Catlow CRA, Rubia TD, Hobbs IW, Kinoshita C, Matzke Hj, Motta AT, Nastasi M, Salie EKH, Vance ER, Zinkle SJ (1998) Radiation effects in crystalline ceramics for the immobilization of high-level nuclear waste and plutonium. J Mater Res 13: 1434–1484

Wengeller H, Martens R, Freund F (1980) Proton conductivity of simple ionic hydroxides. Part II: In situ formation of water molecules prior dehydration. Ber Bunsendes Phys Chem 84: 874–879

Young NA (1999) Mechanisms and kinetics in the solid state. Annu Rep Prog Chem (A) 95: 507–533

Zviagina BB (2000) Modern trends in clay mineral science in Russia and the allied states. Book of Abstracts of the 16th Conference on Clay Mineralogy and Petrology, Karlovy Vary, Czech Republic, August 27th–31st, 2000: 15–17